

IHTC-17 | ID: 0031

LASER HEATING AND MELTING OF METALS ON NANOSCALE: BREAKUP OF METAL FILAMENTS

Ryan H. Allaire¹, Linda J. Cummings ², Lou Kondic^{2*}

¹Department of Mathematical Sciences, United States Military Academy, West Point, NY, 10996, USA ²Department of Mathematical Sciences, New Jersey Institute of Technology, Newark, NJ, 07102, USA

ABSTRACT

We apply a previously-developed asymptotic model to study instability and breakup of metal filaments of nanometric dimensions exposed to heating by laser pulses, and placed on thermally conductive substrates. One particular aspect of this setup is that the considered heating is volumetric, since the absorption length of the applied laser pulse is comparable to a typical filament thickness. In such a setup, absorption of thermal energy and filament evolution are coupled, and must be considered self-consistently. The asymptotic model that we use allows for significant simplification, since it reduces a complicated problem involving Navier-Stokes equations coupled with heat transport. Such simplification is crucial both for understanding the main features of the problem, and for the purpose of developing efficient simulations of the filament evolution and subsequent nanoparticle formation. The presented computational results are obtained in the GPU computing environment, which allows for fully nonlinear time-dependent simulations in large three-dimensional computational domains. We focus in particular on the influence of filament size on the evolution. It is found that filaments' width and thickness play an important role, with thicker and/or wider filaments absorbing more energy and therefore evolving differently from thinner ones. This finding opens the door to considerations of self- and directed-assembly of metal nanoparticles via suitable choice of the initial metal geometry on the nanoscale.

KEYWORDS: Nanofluidics, Laser Heating, Long-wave theory, Thin films, Computational methods, GPU simulations, Metal filaments, Fluid instabilities

1. INTRODUCTION

Metal particles, films, and other geometries characterized by nanoscale dimensions have, in recent years, been considered extensively in a variety of applications. These include plasmonics of relevance to solar cells, catalysis, and biomedical applications among others, as reviewed extensively [1, 2, 3, 4, 5, 6]. Developing such systems on the nanoscale is not trivial and a variety of approaches have been considered, with many researchers in the field considering self and directed assembly one of the most promising. As commented by Makarov *et al.* in a recent review: 'Indeed, a self-assembly process via dewetting of heated thin films is a cost-effective and environment-friendly approach for almost disordered nanostructures fabrication. . . Therefore, development of a method based on lithography-free and single-step dewetting, making possible fabrication of both ordered and disordered nanostructures, would be very prospective for a broad range of plasmonic applications' [4].

In experiments and applications, typically laser pulses are used to bring the metals rapidly above the melting point, to facilitate dynamics on fast (nanoseconds) time scales. Modeling such systems is challenging, since a variety of effects must be included, in particular regarding the coupling of thermal effects due to the laser

*Corresponding Author: kondic@njit.edu

heating (including melting and solidification) with fluid dynamics, as discussed in our recent review [7].

In the present paper, we build upon our previous work for coupling of fluid dynamics with thermal effects [8, 9], which constitutes a self-consistent and asymptotically-accurate framework for a complex problem. The resulting set of equations is discretized and solved in a GPU-based computing environment, using our open-source, publicly available code [10]. Our particular focus is on evolving metal filaments of various sizes; such simple geometry illustrates the importance of careful coupling of the fluid dynamics with thermal transport and provides a rudimentary proof-of-principle of the use of initial metal geometry to control the final droplet (nanoparticle) size and number, without the additional complexities that would be anticipated for more elaborate initial geometries.

2. MODEL

Understanding the role that heat flow plays in the evolution and dewetting of thin nanoscale films is a complicated problem, with a large number of physical effects and complicating factors being potentially relevant. Some examples specific to our study include the very short time scales characterizing the pulsed laser source; phase change and fluid flow leading (ideally) to dewetting and pattern formation; the temperature dependence of physical properties; and accurate description of the heat flow itself. In particular, as will be discussed more precisely below, the relevant time scales of some of the key processes are comparable, and therefore require a self-consistent formulation. This is particularly important for laser-irradiated metals: as the film or pattern height evolves, the heat absorption changes also, leading to a direct coupling between the fluid flow and heat transport processes. Since material parameters such as surface tension and viscosity are also (sometimes strongly) temperature-dependent, we arrive at a complex problem that is very challenging to model and resolve, either analytically or computationally. Given the above, a range of models of varying complexity (and accuracy) can be proposed [7], depending on the degree to which coupling of thermal and fluid mechanical aspects is implemented, how heat flow is modeled, and which additional effects (such as dependence of material parameters on temperature) are included.

In earlier work [11], a quasi-one-dimensional model (1D) for film evolution was studied, where only heat flow in the out-of-plane direction is accounted for. While this can be justified in certain cases, we later showed [12] that inclusion of lateral heat flow can influence results significantly. However, this demonstration involved simulating the full heat diffusion equation with a moving boundary, which has high computational cost and has so far been implemented only for small computational domains. Scaling up to larger 3D domains is neither feasible nor desirable: we need a simplified formulation that will allow us to develop better understanding of the relevance of heat flow, while yet retaining the key physics.

The most complete model consists of the Navier-Stokes equations for the molten metal film, coupled with heat equations for the metal and substrate, plus appropriate boundary conditions and constitutive equations for the temperature-dependent material parameters. In our recent work [8, 9] we formulated a simplified asymptotic model for this setup based on a long wave formulation for a thin metal geometry. The metal film thickness (z = h(x, y, t)) where x and y are the in-plane coordinates) evolution is governed by the following 4th order nonlinear partial differential equation,

$$\partial_t h + \nabla_2 \cdot \left[\frac{1}{\mu(T)} \left(h^3 \nabla_2 \left(\Gamma \nabla_2^2 h + \Pi(h) \right) + h^2 \text{Ma} \nabla_2 \left(\Delta T \right) \right) \right] = 0 \tag{1}$$

where $\nabla_2 = (\partial_x, \partial_y, 0)$. This equation, here given in non-dimensional form, uses typical film thickness in the experiments, H (~10 nm), as the out-of-plane lengthscale, and the wavelength of maximum growth, $\lambda_{\rm m}$, obtained from linear stability analysis of a flat isothermal film, as the in-plane lengthscale, leading to the small aspect ratio $\epsilon = H/L \ll 1$, where $L = \lambda_{\rm m}/(2\pi)$, and $\lambda_{\rm m} \sim 100$ nm. (The instability is due to the destabilizing disjoining pressure, discussed further below and extensively in our earlier works [7, 13].) The time scale is $t_{\rm scl} = 3L\mu_{\rm melt}/(\epsilon^3\gamma_{\rm melt})$ (where $\mu_{\rm melt}$ and $\gamma_{\rm melt}$ are the fluid viscosity and surface tension

at the melting temperature, $T_{\rm melt}$); consistent with the timescale of evolution of melted films, $t_{\rm scl} \approx 20$ ns (exact values depend on the metal considered). Following the time derivative term in Eq. (1), the terms are the capillary, disjoining pressure, and Marangoni terms, respectively. Here, $\mu(T)$ represents temperature-dependent viscosity (scaled by $\mu_{\rm melt}$), Γ is the leading order surface tension (scaled by $\gamma_{\rm melt}$), and Ma is the Marangoni number accounting for variation of surface tension due to temperature gradients at the metal surface, ΔT . The film evolution is coupled to a self-consistent model for the film temperature, which we now outline before discussing Eq. (1) in more detail.

The heat flow model developed in our recent work [8] exploits further the long-wave approximation. The metal has much higher thermal conductivity than the substrate, and the temperature variation across the film (in the short, z-direction) may be shown to be weak. One can then derive a governing equation for the leading-order temperature of the metal film, $T_f(x, y, t)$, given in non-dimensional form as,

Pe
$$h\partial_t T_f = \nabla_2 \cdot (h\nabla_2 T_f) - \mathcal{K} (\partial_z T_s)|_{z=0} + h\overline{Q}.$$
 (2)

The major advantage of this formulation is that the film temperature can be computed self-consistently based on the current value of the film thickness, h, and without carrying out computationally expensive resolution of the temperature in a time-dependent computational domain (determined by the evolving film thickness, h). This type of asymptotic modeling forms the basis for our proposed work. In Eq. (2), the Peclet number is defined by

Pe =
$$(\rho c)_{\text{melt}} \gamma_{\text{melt}} \epsilon^2 H / (3\mu_{\text{melt}} k_{\text{melt}}),$$
 (3)

where $(\rho, c, k)_{\text{melt}}$ are the density, heat capacity, and thermal conductivity of the metal film at the melting temperature, $\mathcal{K} = k_{\text{s}}/(\epsilon^2 k_{\text{melt}})$ is the scaled ratio of thermal conductivities of the substrate and the metal, and T_{s} is the substrate temperature. The last term in the equation is due to laser heating, averaged over the metal thickness,

$$\overline{Q} = h^{-1} \int_0^h F(t) [1 - R(h)] \exp[-\alpha_f (h - z)] dz.$$
 (4)

Here, α_f^{-1} is the dimensionless absorption length for laser radiation in the metal film and F(t) captures the temporal shape of the laser pulse, taken to be Gaussian centered at specified time t_p and of prescribed width σ (measured in tens of nanoseconds in dimensional terms). In general the reflectivity of the film on a transparent substrate, R(h), can be found by solving Maxwell's equations [14], but the resultant form is cumbersome; following [15, 16] we approximate it by

$$R(h) = \left[1 - r_0 \left(1 - \exp\left(-\alpha_{\rm r} h\right)\right)\right] \tag{5}$$

where r_0 and α_r are fitting parameters.

Returning to the film evolution, Eq. (1), the temperature dependence of surface tension enters via the capillary term, reflecting the balance of normal stresses at the metal-air interface, and the Marangoni term, reflecting the tangential stress balance. An asymptotic approach (consistent with the above assumptions) including both spatial and temporal dependence of the surface tension leads to

$$\gamma = \Gamma + \epsilon^2 \frac{2Ma}{3} \Delta T \tag{6}$$

where γ_T specifies the gradient of surface tension with respect to temperature. In general, Γ may depend on average film temperature (normalized by T_{melt}), but for simplicity in the current simulations we use $\Gamma = 1$.

The temperature dependence of viscosity $\mu(T)$ is modeled by an Arrhenius-type relationship,

$$\mu(T) = S(T_{\rm f}) \exp\left(\frac{E}{RT_{\rm melt}} \left(\frac{1}{T_{\rm f}} - 1\right)\right),\tag{7}$$

$$S(T_{\rm f}) = \frac{1}{2} \left(\tanh \left(T_{\rm melt}(T_{\rm f} - 1) + 5 \right) + 1 \right) \tag{8}$$

where R is the universal gas constant, and E is the activation energy [17]. Here, we follow the approach developed in [15] in utilizing Eq. (7). Here, spatial dependence of viscosity is used to for the purpose of melting/solidification control and the Sigmoid function in Eq. (8) is used to sharpen the phase transition.

To close the problem, one needs to couple the thermal problem in the film with the heat transport in the substrate. Solving for the substrate heat flow is straightforward, since the computational domain is fixed: one just needs to specify appropriate boundary conditions. In this work, we assume Dirichlet lateral boundary conditions (specified by substrate temperature T_s at the domain boundary being room temperature), perfect thermal contact at z = 0, and a Newton cooling condition,

$$\partial_z T_s = \text{Bi}(T_s - T_a) \quad \text{at} \quad z = -H_s.$$
 (9)

Here the Biot number is specified by Bi = $\alpha H_{\rm S}/k_{\rm S}$ where α measures the thermal contact between the substrate and the medium below $z=-H_{\rm S}$.

For metal films of nanoscale thickness, instability due to destabilizing metal-substrate interaction is an important effect, since the range of the interaction potential is comparable to the film thickness [18]. This is currently modeled via a disjoining pressure of the form

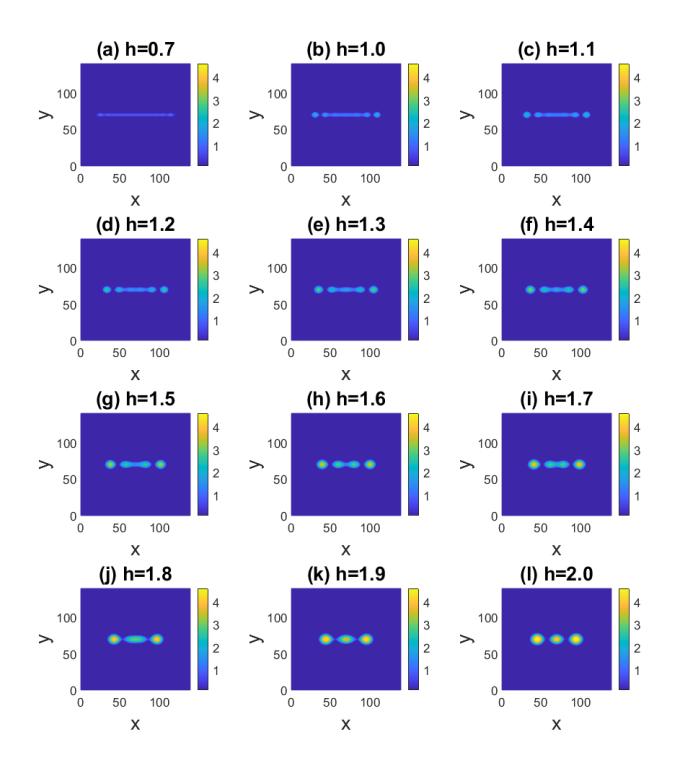
$$\Pi(h) = \kappa [(h_*/h)^n - (h_*/h)^m]$$
(10)

with equilibrium dimensionless film thickness h_* , constant κ (related to the Hamaker constant A by $\kappa = A/(\gamma_{\text{melt}}h_*^3H^2)$), and exponents n > m > 1 [11]. In simulations of the model, such a disjoining pressure term will ensure that the film height nowhere goes to zero, but instead approaches the minimum value h_* as dewetting proceeds (we typically use $h_* = 0.1$, corresponding to 1 nm; while this value is larger than that expected in experiments [13], this choice avoids the numerically more expensive simulations that are required for smaller values of h_*). Interfacial potentials for liquid metals are undoubtedly more complex than specified here, however, based on our earlier body of work and extensive comparison to experiment (see in particular [13]), we expect that the present form is sufficient for our purposes; further details on disjoining pressure models in this context are given in our recent review [7].

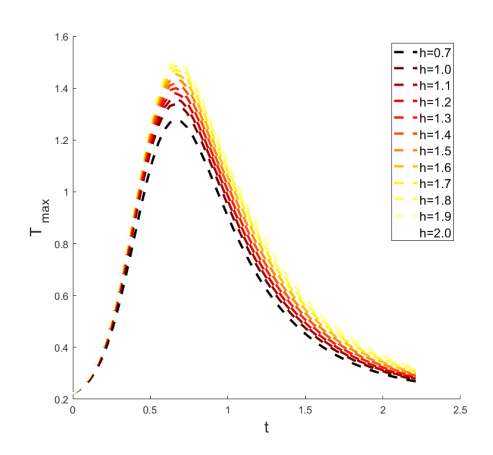
3. RESULTS

In the present paper we focus on setups relevant to recent experiments [19], involving so-called 'membranes'. Membranes are essentially very thin solid substrates with overlaid nanoscale metal patterns, obtained by combining lithographic techniques with chemical etching of the underlying silicon [19]. One important motivation for using membranes is that one is able to observe not only the final outcome of the experiments, but also the time evolution. Such information can be obtained since membranes are optically transparent and allow for the use of dynamic transmission electron microscopy (DTEM), which provides unique nanosecond temporal and nanometer spatial resolution [19]. From the modeling perspective, a key point is that in such a setup, one typically has very small values of the Biot number, Bi, meaning that the bottom boundary of the substrate is essentially insulating. Therefore, the membrane setup allows for precise control of heat flow. Ignoring radiation losses, on the timescale of the experiments heat is lost (in the limit $Bi \rightarrow 0$) only through lateral boundaries, and with an appropriate choice of geometry, such losses could be minimized as well. As a consequence, one can melt the metals with much lower laser pulse energy, and model the thermal field more precisely.

An additional potential simplification when modeling the heat flow for experiments on thin membranes is that the substrate Peclet number Pe_s (defined analogously to the fluid one introduced in Eq. (2)), is typically small. This suggests that, instead of solving a full diffusion problem in the substrate, it is be sufficient to solve a much simpler boundary value problem (BVP) for the temperature. Our results indicate that, for sufficiently thin substrates (such as membranes), the differences in the solutions of the diffusion equation and the BVP for substrate temperature are minimal [8].



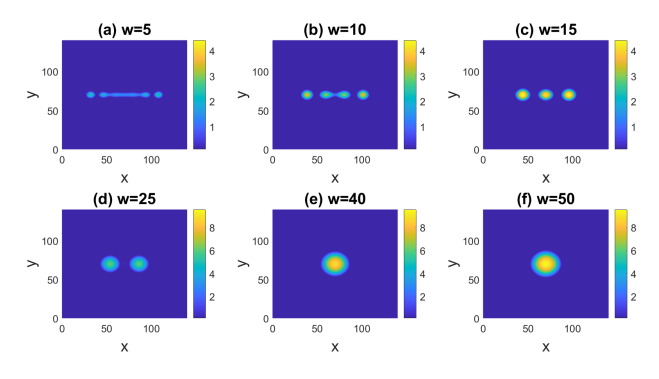
(a) Filaments' final configurations.



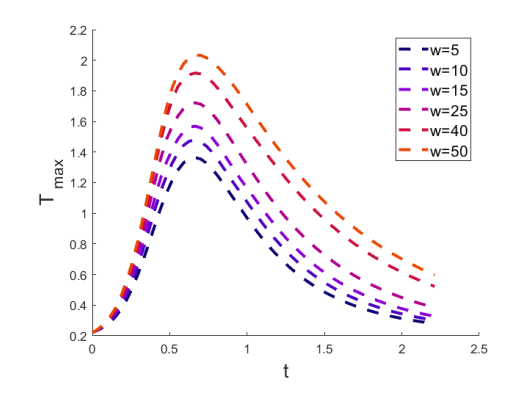
(b) Maximum temperature of the filaments from (a).

Fig. 1 Final metal configurations obtained after applying laser heating to filaments of different initial heights, h. The figure shows the view from above, with the title of each plot showing the maximum initial filament height using non-dimensional units as described in the text. In each of the panels in part (a), the filament width w is four times the height.

Figure 1 shows an example of our computational results, simulating evolution of metal filaments, surrounded by a thin layer whose thickness, h_* , corresponds to the stable thickness resulting from the disjoining pressure, Eq. (10). As mentioned above, for computational reasons, h_* may be assigned a value larger than realistic; see the discussion in Ref. [13]. This becomes relevant due to the form of the heat source term in equation (2), where energy is absorbed by the film according to its local thickness; a too-large value for h_* could



(a) Filaments' final configurations.



(b) Maximum temperature of the filaments from (a).

Fig. 2 Final metal configurations obtained after applying laser heating to filaments of different initial widths, w. The figure shows the view from above, with the title of each plot showing the maximum initial filament width using non-dimensional units as described in the text. In each of the panels in part (a), the filament height h is fixed at h = 1.

lead to overestimates of the local heat absorbed by the film in dewetted regions (where no metal should be present in practice), and potentially inaccurate predictions. We account for this effect by "turning off" the heat absorption term in the part of the domain covered by this equilibrium layer.

The initial condition in the simulation is a metal filament, defined by

$$h(x, y, 0) = h_* + A_0 \left(\tanh(x - x_1) \tanh(x_2 - x) + 1 \right) \left(\tanh(y - y_1) \tanh(y_2 - y) + 1 \right),$$

where $x_1 = 20$ and $x_2 = 120$ are the lateral boundaries of the filament (making a filament of length 100 dimensionless units) and $y_1 = 70 - w/2$, $y_2 = 70 + w/2$ are the transverse boundaries (setting the filament width, w, which we vary in simulations). The scaling factor A_0 determines the height of the filament and is also varied in simulations, as described below. Initially both metal and substrate are assumed to be at room temperature. Then, the laser pulse is applied, the metal temperature increases (discussed more precisely in what follows) and, when the filament temperature rises above the melting point, it starts evolving as a Newtonian fluid. When the laser energy begins to decrease, the filament temperature decreases also, and once it drops below the melting temperature, the evolution stops. Figure 1 shows the final result of this process.

The simulations are carried out using our in-house previously developed GPU-based code [10]. The computational method itself is based on finite difference spatial discretization, combined with Crank-Nicolson temporal evolution within an ADI (alternate direction implicit) framework; see [9] for details.

Figure 1, part (a) shows that filaments of different initial height evolve differently. Thin filaments (see, e. g. panel (a) in part (a)) do not absorb enough heat and barely melt; we discuss filament temperatures in more detail in what follows. As filament thickness increases, the amount of absorbed energy increases as well; the filaments spend more time in the liquid phase, and therefore instabilities have more time to develop. For the present configuration, the behavior observed in Fig. 1 part (a) involves 'beading' or 'pearling' type instabilities, which propagate from the filament ends [20]. Such propagation takes time, and therefore longer liquid lifetimes allow instabilities to propagate further towards the center of the filament.

Figure 1, part (b) shows the maximum temperature of the filaments from Fig. 1, part (a) as a function of (non-dimensional) time. This figure confirms that thicker filaments become hotter, and their temperature is above melting for a longer period of time. Both effects are relevant from the viewpoint of filament dynamics: higher temperatures lead to lower viscosity and therefore faster evolution, and longer liquid lifetimes allow a filament to evolve for a longer time.

Figure 2, part (a) shows that it is not only the initial filament height that matters, but also the width. The main reason for this is that more energy is absorbed for wider filaments; in addition, once the filament melts, it contracts into a structure resembling part of a cylinder. Wider filaments will lead to larger cylinders, increasing the energy absorption even further. This is also reflected in Figure 2, part (b), which shows the maximum temperature of the filaments from part (a).

4. CONCLUSIONS

In this paper, we have illustrated a simple but powerful method that allows for coupling of fluid dynamics and heat transport for metal filaments deposited on thermally conductive substrates. Our approach is fully self-consistent, with fluid dynamics both influencing and being influenced by the heat flow. This coupling occurs through temperature dependence of material parameters, in particular metal viscosity and surface tension, which influence the fluid thickness, which in turn influences the amount of heating absorbed. In the present work, we apply this method to metal filaments; however in principle the model can be used for any material and any initial material geometry exposed to volumetric heating. In the context of metals, our results open the door to various directed- and self-assembly approaches, since it is possible to control the dynamics by specifying desired initial geometries.

ACKNOWLEDGMENT

This research was supported by NSF DMS-1815613 and by an NJIT seed funding grant (2022).

NOMENCLATURE

Table 1 provides the values of the dimensional parameters used, and Table 2 the derived dimensionless quantities.

Parameter	Notation	Value	Unit
Viscosity at T _{melt}	$\mu_{ m melt}$	4.3×10^{-3}	Pas
Surface tension at T_{melt}	$\gamma_{ m melt}$	1.303	Jm ⁻²
Wavelength of maximum growth	$\lambda_{\rm m}$	180.84	nm
Vertical length scale	$\mid H \mid$	10	nm
Horizontal length scale	$L = \lambda_{\rm m}/(2\pi)$	28.78	nm
Time scale	$t_{\rm scl} = 3L\mu_{\rm melt}/(\epsilon^3\gamma_{\rm melt})$	6.79	ns
Melting Temperature	$\mid T_{ m melt}$	1358	K
Film density	$ ho_{ m melt}$	8000	kgm ⁻³
SiO ₂ density	$\mid ho_{ extsf{s}}$	2200	kgm ⁻³
Film specific heat capacity	$c_{ m melt}$	495	Jkg ⁻¹ K ⁻¹
SiO ₂ specific heat capacity	$c_{\rm s}$	937	$ $ Jkg $^{-1}$ K $^{-1}$
Film heat conductivity	$k_{ m melt}$	340	$\mid \mathrm{Wm^{-1}K^{-1}}\mid$
SiO ₂ heat conductivity	$k_{\rm s}$	1.4	$ Wm^{-1}K^{-1} $
Film absorption length	$\mid \alpha_{ m f}^{-1} H \mid$	11.09	nm
Temp. Coeff. of Surf. Tens.	$\gamma_{ m T}$	-0.23×10^{-3}	$J m^{-2} K^{-1}$
Hamaker constant	A	3.49×10^{-17}	J
Reflective coefficient	$\mid r_0 \mid$	0.3655	1
Film reflective length	$\alpha_{\rm r}^{-1}H$	12.0	nm
Laser energy density	$\mid E_0 \mid$	760	Jm ⁻²
Gaussian pulse peak time	$t_{\rm p} t_{\rm scl}$	12	ns
Equilibrium film thickness	$\mid h_*H$	1	nm
Mean filament thickness	$\mid h_0 H$	7 - 20	nm
Filament widths	$\mid wH$	5 - 50	nm
SiO ₂ thickness	$H_{\rm s}H$	15	nm
Room temperature	$T_a T_{\text{melt}}$	300	K
SiO ₂ Heat Transfer Coefficient	α	0	$ Wm^{-2}K^{-1} $
Activation Energy	$\mid E \mid$	30.5	kJ mol ⁻¹

Table 1 Parameters used for simulations. Taken from [9].

Dimensionless Numbers	Notation	Value	Expression
Aspect Ratio	ϵ	0.347	H/L
Film Peclet Number	Pe	1.42×10^{-3}	$(\rho c)_{\mathrm{melt}} \gamma_{\mathrm{melt}} \epsilon^2 H / (3 \mu_{\mathrm{melt}} k_{\mathrm{melt}})$
Biot Number	Bi	0	$\alpha_{ m s}H/k_{ m s}$
Thermal Conductivity Ratio	\mathscr{K}	0.034	$k_{\rm s}/(\epsilon^2 k_{ m melt})$
Range of Dimensionless Viscosity	\mathcal{M}	0.028 - 1	$\mu/\mu_{ m melt}$
Marangoni Number	Ma	0.35	$3\gamma_{ m T}T_{ m melt}/(2\gamma_{ m melt})$

Table 2 Dimensionless parameters based on material parameters in Table 1.

REFERENCES

- [1] Atwater, H. and Polman, A., "Plasmonics for improved photovoltaic devices", Nature Materials, 9, p. 9 (2010).
- [2] Wang, D. and Li, Y., "Bimetallic nanocrystals: Liquid-phase synthesis and catalytic applications", *Advanced Materials*, 23, pp. 1044–1060 (2011).
- [3] Chaudhuri, R. G. and Paria, S., "Core/shell nanoparticles: Classes, properties, synthesis mechanisms, characterization, and applications", *Chemical Reviews*, 112, pp. 2373–2433 (2012).
- [4] Makarov, S. V., Milichko, V. A., Mukhin, I. S., Shishkin, I. I., Zuev, D. A., Mozharov, A. M., Krasnok, A. E. and Belov, P. A., "Controllable femtosecond laser-induced dewetting for plasmonic applications", *Laser Photonics Rev.*, 10, p. 91 (2016).
- [5] Hughes, R. A., Menumerov, E. and Neretina, S., "When lithography meets self-assembly: a review of recent advances in the directed assembly of complex metal nanostructures on planar and textured surfaces", *Nanotechnology*, 28, p. 282002 (2017).

- [6] Ruffino, F. and Grimaldi, M. G., "Nanostructuration of Thin Metal Films by Pulsed Laser Irradiations: A Review", *Nanomaterials*, 9, p. 1133 (2019).
- [7] Kondic, L., González, A. G., Diez, J. A., Fowlkes, J. D. and Rack, P., "Liquid-State Dewetting of Pulsed-Laser-Heated Nanoscale Metal Films and Other Geometries", *Annu. Rev. Fluid Mech.*, 52, p. 235 (2020).
- [8] Allaire, R. H., Cummings, L. J. and Kondic, L., "On efficient asymptotic modelling of thin films on thermally conductive substrates", *J. Fluid Mech.*, 915, p. A133 (2021).
- [9] Allaire, R. H., Cummings, L. J. and Kondic, L., "Influence of thermal effects on the breakup of thin films of nanometric thickness", *Phys. Rev. Fluids*, 7, p. 064001 (2022).
- [10] Allaire, R. H., "GADIT THERMAL", https://github.com/Ryallaire/GADIT_THERMAL (2021).
- [11] Dong, N. and Kondic, L., "Instability of nanometric fluid films on a thermally conductive substrate", *Phys. Rev. Fluids*, 1, p. 063901 (2016).
- [12] Seric, I., Afkhami, S. and Kondic, L., "Direct numerical simulation of variable surface tension flows using a Volume-of-Fluid method", J. Comput. Phys., 352, p. 615 (2018).
- [13] González, A., Diez, J. A., Wu, Y., Fowlkes, J. D., Rack, P. D. and Kondic, L., "Instability of liquid Cu films on a SiO2 substrate", *Langmuir*, 29, p. 9378 (2013).
- [14] Heavens, O., *Optical Properties of Thin Solid Films*, Dover books on physics and mathematical physics, Dover Publications (1955).
- [15] Seric, I., Afkhami, S. and Kondic, L., "Influence of thermal effects on stability of nanoscale films and filaments on thermally conductive substrates", *Phys. Fluids*, 30, p. 012109 (2018).
- [16] Trice, J., Thomas, D., Favazza, C., Sureshkumar, R. and Kalyanaraman, R., "Pulsed-laser-induced dewetting in nanoscopic metal films: Theory and experiments", *Phys. Rev. B*, 75, p. 235439 (2007).
- [17] Gale, W. and Totemeier, T., Smithells Metals Reference Book (Eighth Edition), Butterworth-Heinemann (2004).
- [18] Israelachvili, J. N., Intermolecular and surface forces, New York: Academic Press, second edition (1992).
- [19] Diez, J., González, A., Garfinkel, D., Rack, P., McKeown, J. and Kondic, L., "Simultaneous Decomposition and Dewetting of Nanoscale Alloys: A Comparison of Experiment and Theory", *Langmuir*, 37, p. 2575 (2021).
- [20] Diez, J. A., González, A. and Kondic, L., "On the breakup of fluid rivulets", Phys. Fluids, 21, p. 082105 (2009).